The International Journal of Cardiovascular Imaging (2019) 35:1563–1572
https://doi.org/10.1007/s10554-019-01611-y

ORIGINAL PAPER

Simultaneous evaluation of plaque stability and ischemic potential of coronary lesions in a fluid–structure interaction analysis

Xinlei Wu[1,2] · Clemens von Birgelen[3] · Su Zhang[1,2] · Daixin Ding[1,2] · Jiayue Huang[1,2] · Shengxian Tu[1,2]

Received: 23 March 2019 / Accepted: 23 April 2019 / Published online: 3 May 2019

Abstract

The measurement of fractional flow reserve (FFR) and superficial wall stress (SWS) identifies inducible myocardial ischemia and plaque vulnerability, respectively. A simultaneous evaluation of both FFR and SWS is still lacking, while it may have a major impact on therapy. A new computational model of one-way fluid–structure interaction (FSI) was implemented and used to perform a total of 54 analyses in virtual coronary lesion models, based on plaque compositions, arterial remodeling patterns, and stenosis morphologies under physiological conditions. Due to a greater lumen dilation and more induced strain, FFR in the lipid-rich lesions (0.81 ± 0.15) was higher than that in fibrous lesions (0.79 ± 0.16, $P = 0.001$) and calcified lesions (0.79 ± 0.16, $P = 0.001$). Four types of lesions were further defined, based on the combination of cutoff values for FFR (0.80) and maximum relative SWS (30 kPa): The level of risk increased from (1) plaques with mild-to-moderate stenosis but negative remodeling for lipid-rich (Type A: non-ischemic, stable) to (2) lipid-rich plaques with mild-to-moderate stenosis and without-to-positive remodeling (Type B: non-ischemic, unstable) or plaques with severe stenosis but negative remodeling for lipid-rich (Type C: ischemic, stable) to (3) lipid-rich plaques with severe stenosis and without-to-positive remodeling (Type D: ischemic, unstable). The analysis of FSI to simultaneously evaluate inducible myocardial ischemia and plaque stability may be useful to identify coronary lesions at a high risk and to ultimately optimize treatment. Further research is warranted to assess whether a more aggressive treatment may improve the prognosis of patients with non-ischemic, intermediate, and unstable lesions.

Keywords Plaque stability · Myocardial ischemia · Fractional flow reserve · Fluid–structure interaction · Cardiovascular biomechanics

Abbreviations

CFD	Computational fluid dynamics
DS%	Percent diameter stenosis
FEA	Finite element analysis
FFR	Fractional flow reserve
FSI	Fluid–structure interaction
MLD	Minimum lumen diameter
rSWS	Relative superficial wall stress

Electronic supplementary material The online version of this article (https://doi.org/10.1007/s10554-019-01611-y) contains supplementary material, which is available to authorized users.

✉ Shengxian Tu
sxtu@sjtu.edu.cn

[1] Biomedical Instrument Institute, School of Biomedical Engineering, Shanghai Jiao Tong University, Shanghai, China

[2] Shanghai Med-X Engineering Research Center, Shanghai Jiao Tong University, Shanghai, China

[3] Thoraxcentrum Twente, Medisch Spectrum Twente, Enschede, The Netherlands

Introduction

The potential of a certain lesion to induce myocardial ischemia as well as the underlying vulnerability of the plaque are two important issues that are considered by clinicians when deciding whether there is a need for coronary revascularization. Measurement of fractional flow reserve (FFR) is the current gold standard for assessing whether a particular coronary lesion is hemodynamically significant and may cause myocardial ischemia during physical activity [1–3]. Currently, several novel methods have been developed to non-invasively evaluate FFR, using image information from coronary computed tomography [1, 4] or coronary angiography [5]. However, coronary plaques with different internal composition deform differently in response to the

same blood pressures, with soft lipid-rich plaques presenting the greatest deformation and the most significant changes in lumen diameter [6]. As computational fluid dynamics (CFD)-based technologies usually treat the dynamic lumen as a stationary wall, such approaches are unable to analyze the time-varying hemodynamic states with the dynamic lumen stenosis severity during the cardiac cycle. Therefore, while the impact of plaque composition on FFR is greatly unknown, it may represent a source of error for the non-invasive measurement of FFR.

Approaches that use image-based finite element analysis (FEA) allow to analyze the dynamic nature of coronary lesions geometry in order to assess the risk of plaque rupture [6–12]. Patient-specific image-based FEA studies have shown that plaques with a higher fibrous cap/wall stress are prone to rupture and might induce acute coronary events [7–9], while the maximum cap stress or superficial wall stress (SWS) may serve as a biomechanical predictor of plaque vulnerability [10–13]. However, the mechanical environment of a coronary plaque is a highly complex interaction process, in which the change of coronary arterial wall morphology, caused by cardiac contraction, can alter intraluminal blood flow domains and hemodynamic parameters (e.g., flow velocity, blood pressure), that in turn can react on the vessel wall and affect mural deformation and stress. Previous studies have used the simulations of fluid–structure interaction (FSI) to improve the accuracy identification of vulnerable sites of carotid or coronary plaques [14–16]. However, a simultaneous evaluation of both, inducible myocardial ischemia and plaque vulnerability, is still lacking.

The simultaneous evaluation of the two '*mechanophysiology*' indices FFR and maximum SWS, which respectively characterize the pathophysiological function and biomechanical properties of an individual coronary lesion, might theoretically help tailor treatment of individual coronary lesions. Therefore, in the present study, a one-way FSI computational model was implemented on idealized coronary plaque models with various combinations of plaque tissue, vascular remodeling, and stenosis morphology, in order to assess the impact of the aforementioned lesion features on FFR and maximum SWS.

Materials and methods

Coronary plaque structure and flow models

For coronary plaque structural models, a total of 18 geometric models of coronary plaques were created based on the combination of 3 arterial remodeling patterns (negative, without, and positive remodeling), 3 percent diameter stenoses (DS%) (33.3, 50 and 66.7%) and 2 lesion lengths (10 mm and 20 mm) (Fig. 1A). Plaque burden, plaque volume divided by stenotic segment volume, increased from negative to positive remodeling to resemble the situation in vivo (Fig. 1B). Three scenarios of dissimilar predominant plaque compositions (lipid-rich, fibrous, and calcified plaques) were further created by modifying the corresponding material properties of the plaque compositions. Details of finite element models for all cases have been previously described, including geometric dimensions, mesh density, material parameters of intima, media, and adventitia, and plaque compositions [6].

For intraluminal fluid models, six geometric models were created based on the two lumen shape controlling parameters (i.e., DS% and lesion length). Blood flow in coronary arteries was simulated in a Navier–Stokes model and considered as incompressible, viscous Newtonian fluid with a density of 1060 kg/m^3 and dynamic viscosity of 0.0035 Pa·s. The fluid geometric models for all cases were meshed within ICEM software (v15.0, ANSYS Inc., Canonsburg, Pennsylvania). Boundary layer grids in near wall were generated as follows: the first layer length of 0.0064 mm was calculated by the empirical formula $y = \frac{y^+ \mu}{\rho u^*}$, where the empirical parameter y^+ was 1 for laminar flow model, μ was dynamic viscosity, u^* was friction velocity in near wall, which was calculated by $u^* = \frac{\tau_w}{\rho}$, here, τ_w was wall shear stress. For near wall with boundary layer, a pentahedral mesh of boundary layer with a total height of 0.073 mm was generated by exponential growth with a length ratio of 1.2. The middle part of the blood stream was discretized with a coarser mesh using the following parameters: global element scaling factor of 1, global element length of 1.2 mm, adaptive mesh refinement length of 0.6 mm and refinement factor of 10.

Boundary conditions

For the boundary conditions of fluid models, the proximal pulse pressure (Fig. 2A) and distal flow velocity (Fig. 2B) within one cardiac cycle, measured in a narrowed coronary artery at maximum hyperemia by the pressure transducer of the guiding catheter and Doppler wire respectively [17], were implemented into FLUENT software (v15.0, ANSYS Inc., Canonsburg, Pennsylvania) by use of user defined function.

For structural models, both the proximal and distal ends were constrained in the vessel longitudinal direction, and the outer surface of surrounding tissue was fully constrained. One-way coupling method from structure domain to fluid domain was used instead of two-way FSI to reduce computational efforts. In order to make the lumen deformation within a physiological range, a relative pressure field varied with time and space was performed to apply on the lumen, because wall strain would be significantly overestimated under physiological loadings if neglecting residual

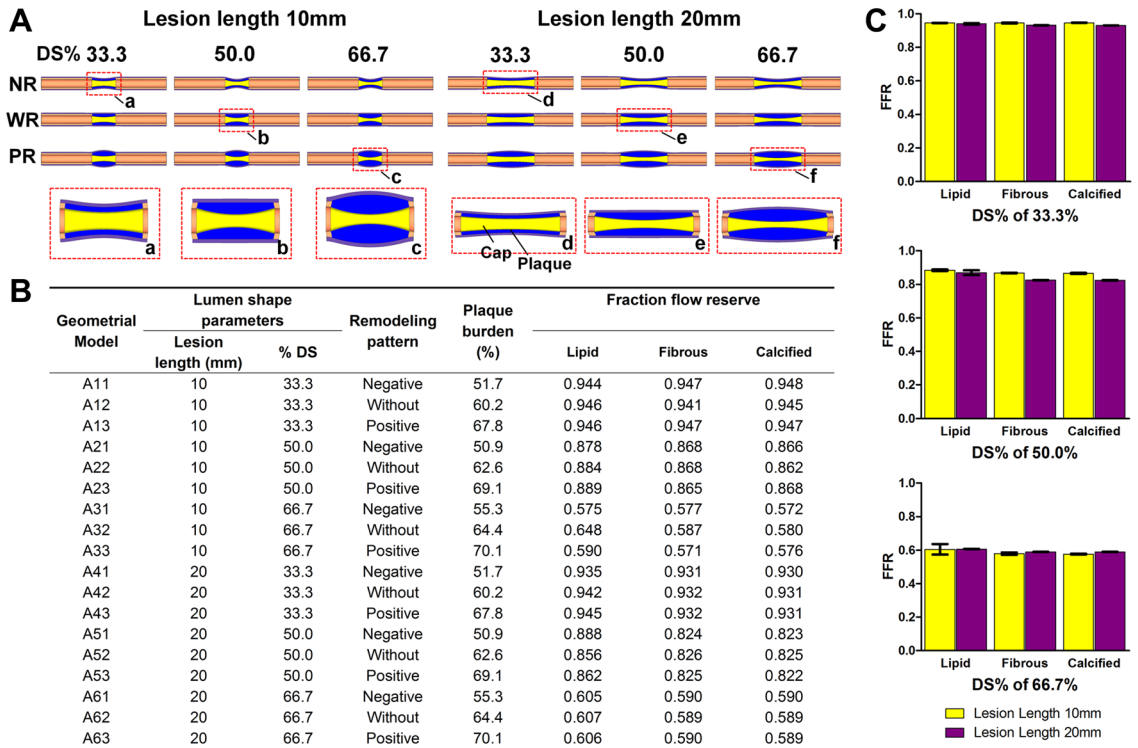

B

Geometrial Model	Lumen shape parameters		Remodeling pattern	Plaque burden (%)	Fraction flow reserve		
	Lesion length (mm)	% DS			Lipid	Fibrous	Calcified
A11	10	33.3	Negative	51.7	0.944	0.947	0.948
A12	10	33.3	Without	60.2	0.946	0.941	0.945
A13	10	33.3	Positive	67.8	0.946	0.947	0.947
A21	10	50.0	Negative	50.9	0.878	0.868	0.866
A22	10	50.0	Without	62.6	0.884	0.868	0.862
A23	10	50.0	Positive	69.1	0.889	0.865	0.868
A31	10	66.7	Negative	55.3	0.575	0.577	0.572
A32	10	66.7	Without	64.4	0.648	0.587	0.580
A33	10	66.7	Positive	70.1	0.590	0.571	0.576
A41	20	33.3	Negative	51.7	0.935	0.931	0.930
A42	20	33.3	Without	60.2	0.942	0.932	0.931
A43	20	33.3	Positive	67.8	0.945	0.932	0.931
A51	20	50.0	Negative	50.9	0.888	0.824	0.823
A52	20	50.0	Without	62.6	0.856	0.826	0.825
A53	20	50.0	Positive	69.1	0.862	0.825	0.822
A61	20	66.7	Negative	55.3	0.605	0.590	0.590
A62	20	66.7	Without	64.4	0.607	0.589	0.589
A63	20	66.7	Positive	70.1	0.606	0.590	0.589

Fig. 1 Demonstration of FFR changes according to lesion length, percent diameter stenosis, arterial remodeling pattern and plaque compositions in idealized models. **A** Half section view of 18 structural models of coronary plaques were created based on the combination of lesion length, DS% and arterial remodeling. (a–f) Zoom views of these stenosis segments, yellow color: fibrous cap; blue color: plaque compositions. **B** Parameters for the 18 structural models with 2 lesion lengths (10 and 20 mm), 3 DS% (33.3, 50.0 and 66.7%), and 3 arterial remodeling states (negative, without and positive remodeling). Plaque burden of the models increased from negative to positive remodeling. FFR in lipid-rich lesions (0.81 ± 0.15) was higher than in fibrous (0.79 ± 0.16, $P = 0.001$) and calcified lesions (0.79 ± 0.16, $P = 0.001$). **C** Effects of plaque features on FFR. (Top) DS% of 33.3%; (middle) DS% of 50.0%; (Bottom) DS% of 66.7%; yellow bar: lesion length of 10 mm; violet bar: lesion length of 20 mm. *DS%* percent diameter stenosis, *NR* negative remodeling, *WR* without remodeling, *PR* positive remodeling

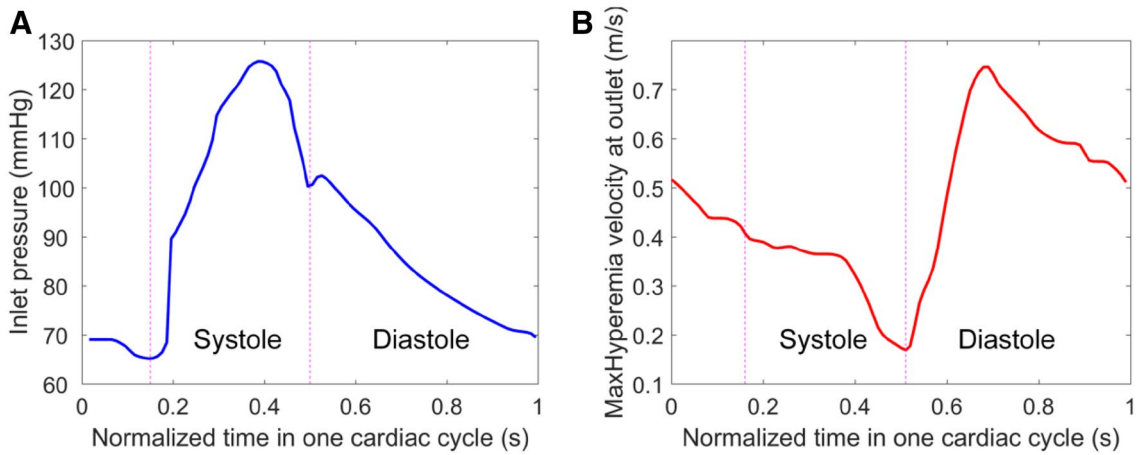

Fig. 2 The boundary conditions of intraluminal blood flow are measured from a patient moderate stenosis at maximum hyperaemia (from Marques et al. [17] with permission). **A** Pressure–time curve at proximal, **B** velocity–time curve at distal

stress [18]. The relative pressure field was obtained as follow: first multiplied the proximal pulse pressure–time curve by the local scaling factors along the vessel, which were obtained by the normalization of the longitudinal pressure drop curve by reference to the proximal pressure [6], and then subtracted the pressure value at initial state. Note that the stress obtained under the relative pressure field was lowered, hereafter noted as relative stress.

End-diastasis (i.e. the phase of near-quiescence in mid-diastole) was selected as the initial time, because the strain energy and stress might be at the lowest level throughout the cardiac cycle. Thus, the systolic time interval ranges from 0.15 to 0.50 s, and the diastolic time interval ranges from 0.50 to 1.0 s and then from 0.0 to 0.15 s.

Fluid–structure interaction solvers

The structural analysis was performed in the commercial finite element software ABAQUS/Explicit (V6.13, Simulia Dassault Systems, Providence, RI, USA), and FLUENT software was used for fluid simulation. In this study, the lowest Reynolds number was around 2044 for the stenosis model with a DS% of 33.3%. Despite the low Reynolds number, turbulence might occur downstream of the stenosis and thus the Standard k-epsilon model was applied for turbulent flow analyses in FLUENT. The real-time data transfer of the nodal positions on the interface from structure to fluid was conducted in MpCCI software (v4.4, Fraunhofer Gesellschaft, München, Germany), which has been extensively used to study FSI phenomenon in various fields [19].

Catheter-derived pressure is generally like to represent total pressure (the sum of static pressure and dynamic pressure), while the pressure computed in FLUENT is static pressure. Thus, it needed to add the item of the dynamic pressure $\frac{1}{2}\rho v^2$ for FFR calculation, especially in the stenotic segment with a quadratic increase in dynamic pressure due to substantial increase of blood flow velocity at the stenosis [20].

Mechanophysiology indices of coronary plaques

A previous study suggests that plaque structural stress value of 135 kPa is a good predictor of rupture in higher risk regions [21]. However, Ohayon et al. indicates that peak stress may be overestimated by approximately four-folds, if residual stress is neglected [18]. Thus, we set 30 kPa as the threshold value of the relative superficial wall stress (rSWS) to determine plaque stability or rupture risk. Lesions with a maximum rSWS > 30 kPa were plaques with low stability, otherwise, plaques had high stability. Moreover, to determine the ischemia-causing property of lesions, we used an FFR threshold of ≤ 0.80, as applied in clinical practice.

Statistics analysis

Descriptive statistics are reported as mean ± standard deviation. Normal distribution was tested with the Shapiro–Wilk test. Differences in FFR between lipid-rich and fibrous, calcified groups were evaluated by Student *t* test or Mann–Whitney *U* test, as appropriate. To investigate the association of the mechanophysiology indices with plaque feature variables (including plaque compositions, plaque burden, DS% and lesion lengths), multivariable regression analysis was performed. These four variables were then considered for entry in the respective multivariable regression models (if $P < 0.1$ in the univariate regression analysis); variables that were no longer significant in this multivariable model were removed from the model using a backward-stepping algorithm. A Kruskal–Wallis H test was used for comparing three groups of plaque compositions. Statistical significance was further examined by post hoc testing to determine paired differences of three plaque composition groups, using Bonferroni correction to account for multiple tests. All statistical tests were two-sided and a $P < 0.05$ was considered statistically significant, except the Bonferroni-adjusted *P* values. All analyses were performed with IBM SPSS (v22.0, SPSS Inc., Chicago, Illinois).

Results

A total of 54 FSI analyses were performed, using the devised idealized stenosis models based on 3 plaque compositions, 3 remodeling patterns, 3 DS%, and 2 lesion lengths.

Transient analysis of fluid structure interaction

A representative example of FSI analysis of the 10 mm-long, a 50% diameter stenosis, and lipid-rich plaque without arterial remodeling is shown in Fig. 3 as well as in Videos 1 and 2. By the 4 key time instants (i.e. end-diastole, mid-systole, end-systole, and mid-diastole), the entire cardiac cycle was divided into 4 periods: early systole, late systole, early diastole, and late diastole. During systole, the peak stress of the lipid-rich plaque first increased to a maximum value of 35.77 kPa at mid-systole (Fig. 3a2), and it then began to decrease (Fig. 3a2–a3). Subsequently, the peak stress retained at a relatively low level during diastole (Fig. 3a3–a4–a1).

Figure 3b1–b4 shows the velocity profiles at 5 mm-intervals along the vessel at the four cardiac phases. At end-systole (t = 0.50 s), the peak flow velocity in the stenotic segment rapidly decreased to a minimum value of 0.63 m/s within 0.10 s (Fig. 3b3); then it sharply increased to a maximum of 3.21 m/s at mid-diastole (t = 0.70 s) (Fig. 3b4). In late diastole, the peak flow velocity began to gradually

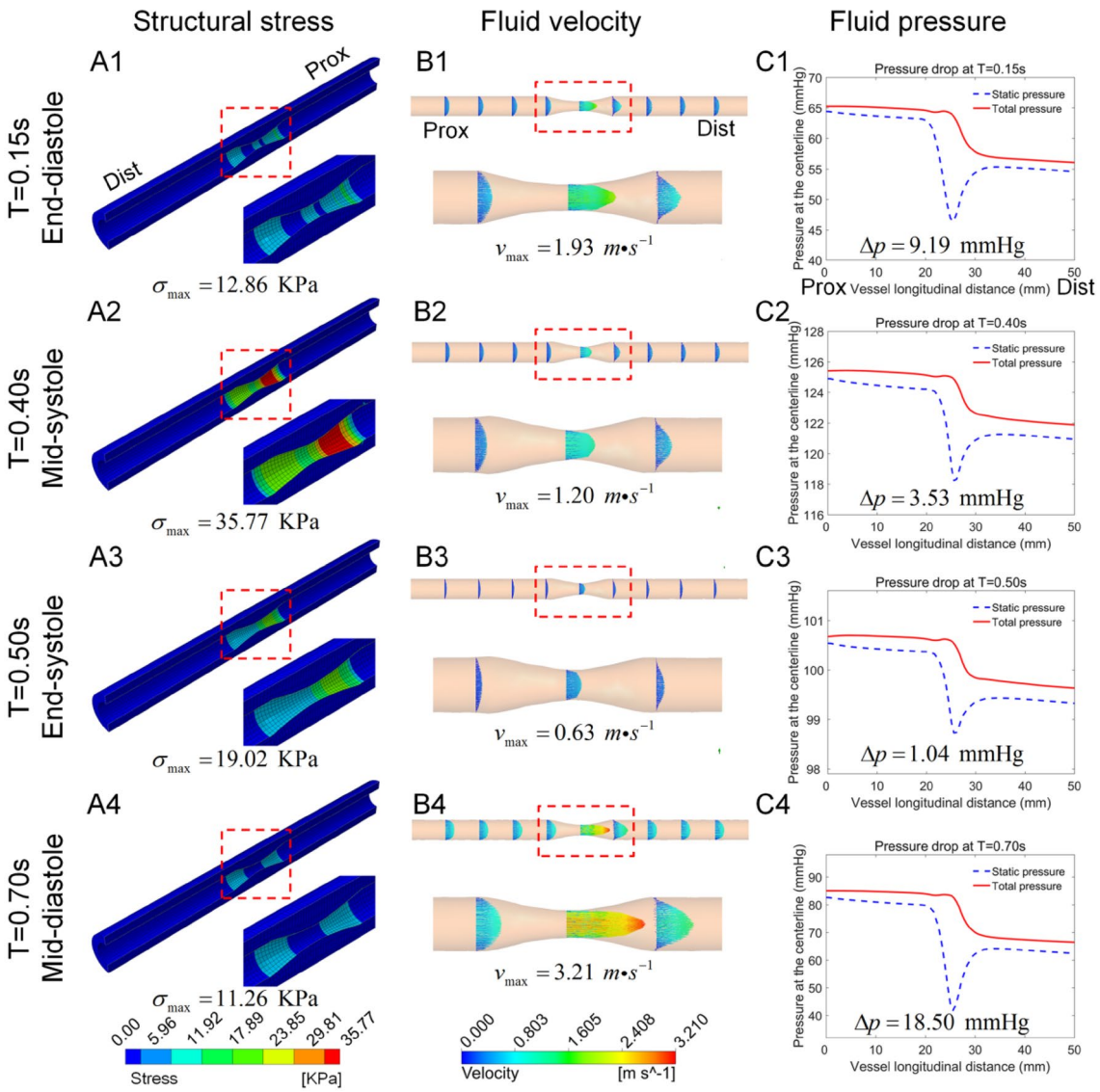

Fig. 3 Representative example of fluid–structure interaction analysis of 10 mm-long lipid-rich plaque with 50% diameter stenosis and without arterial remodeling. **a1–a4** Half section view of structural stress distribution contours, **b1–b4** fluid velocity profiles at 5 mm-intervals in the lumen, **c1–c4** pressure curves along the vessel longitudinal direction (red solid line: total pressure, blue dotted line: static pressure) at end-diastole (t = 0.15 s), mid-systole (t = 0.40 s), end-systole (t = 0.50 s), mid-diastole (t = 0.70 s) in the cardiac cycle. Prox: Proximal; Dist: Distal. (Videos in online appendix)

decline until mid-systole (Fig. 3b2). As shown in Video 2, the interface of the lipid plaque produced clearly visible deformation due to the dynamic blood pressure, and it thereby altered the DS% and flow velocity.

The dynamic pressure, which is the difference between total pressure (red solid line) and static pressure (blue dotted line) (Fig. 3c1–c4), was first increased then decreased along the vessel's longitudinal axis. And the dynamic pressure reached to a maximum value at the narrowest site for all cardiac phases. Moreover, pressure drop, calculated by subtracting the total pressure of the distal end from that of the proximal end, showed a trend similar to the variation of the peak flow velocity during cardiac cycle. At end-systole, the pressure drop rapidly decreased to a minimum value of 1.04 mmHg (Fig. 3c3), and at mid-diastole it sharply increased to a maximum of 18.50 mmHg (Fig. 3c4). In late diastole, the pressure drop began to decline until mid-systole (Fig. 3c2).

Effect of plaque feature variables on FFR

FFR values were higher in lesions with lipid-rich plaques (0.81 ± 0.15) as compared to FFR values in lesions with fibrous plaques (0.79 ± 0.16, $P = 0.001$) or calcified plaques

(0.79 ± 0.16, $P = 0.001$) (Fig. 1B). Specifically, in the 20 mm-long lesion with a DS% of 33.3% and no artery remodeling, FFR was 0.94, 0.93, and 0.93 for lipid-rich, fibrous, and calcified plaques, respectively. FFR decreased to 0.86, 0.83, and 0.82, respectively, when the DS% increased to 50%. FFR further decreased to 0.61, 0.59, and 0.59, when the DS % increased to 66.7%. Accordingly, in the 20 mm-long lesion without artery remodeling, the difference in minimal lumen diameter (MLD) between lipid-rich and calcified plaques was 0.48 mm when the DS% was 33.3%. The difference in MLD increased to 0.58 mm when the DS% increased to 50%. However, when the DS% further increased to 66.7%, the difference in MLD decreased to 0.03 mm. Of note, the variation in FFR among three plaque compositions was greatest for the DS % of 50% (Fig. 1C middle), and the mean difference in FFR between lipid-rich and calcified plaques was 0.04 in the 20-mm long lesion and 0.02 in the 10 mm-long lesion.

The FFR values of the 20 mm-long plaques were lower than that of 10 mm-long plaques with DS % of 33.3% and 50% (Fig. 1C top and middle, yellow bar vs. violet bar), but were slightly higher than that of 10 mm-long plaques with a DS% of 66.7% (Fig. 1C bottom, yellow bar vs. violet bar). Plaque burden had little influence on the FFR. As may be expectedly, FFR decreased with increasing DS% (Fig. 1C top vs. middle vs. bottom).

Statistical analysis of mechanophysiology indices

DS% was the only independent predictor of FFR (Table 1, Fig. 4B). The variation amplitude of DS% within the cardiac cycle was independently associated with plaque composition and DS% (Table 1). The variation amplitude of DS% in the lipid-rich plaques (0.12% ± 0.09%) was significantly higher than that in fibrous plaques (0.01% ± 0.01%, adjusted $P < 0.001$), and in calcified plaques (0.01% ± 0.00%, adjusted $P < 0.001$) (Fig. 4A). Similar results were obtained for the maximum rSWS among 3 groups of plaque compositions (Fig. 4C). The maximum rSWS was independently associated with both plaque composition and plaque burden (Table 1, Fig. 4C).

Plaque stability and ischemic potential of coronary lesions

Based on the cutoff values of maximum rSWS and FFR, all plaques were graded into 4 categories (Fig. 5). Type A: FFR-negative and low maximum rSWS plaques (FFR > 0.80

Table 1 Independent factors of the mechanophysiology indices of coronary plaques by fluid–structure interaction analysis (n = 54)

Mechanophysiology indices	Independent predictors	Regression coefficients (95% CI)	*P*
FFR	DS %	− 0.175 (− 0.190, − 0.159)	< 0.001
Amplitudes of DS%	Plaque composition	− 0.054 (− 0.072, − 0.037)	< 0.001
	DS %	− 0.028 (− 0.045, − 0.011)	0.002
Maximum rSWS	Plaque composition	− 16.364 (− 19.608, − 13.120)	< 0.001
	Plaque burden	5.063 (1.820, 8.307)	0.003

DS% is the only independent predictor of FFR

Variables entered in the multivariable model: (A) amplitudes of DS%: plaque composition and DS%; (B) maximum rSWS: plaque composition and plaque burden

CI confidence interval, *DS%* percent diameter stenosis, *FFR* fractional flow reserve, *rSWS* relative superficial wall stress

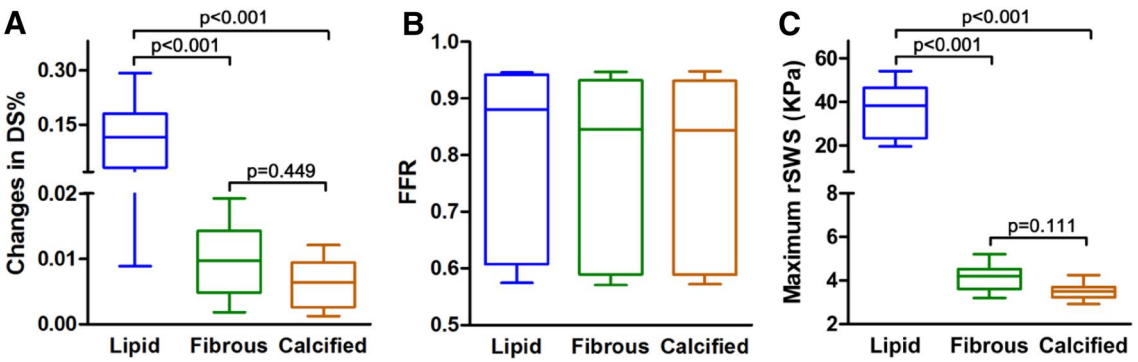

Fig. 4 Effect of plaque compositions on the outcomes of fluid–structure interaction analysis (n = 54). **A** The amplitude of DS% variation, **B** fraction flow reserve (FFR), **C** maximum relative superficial wall stress (rSWS)

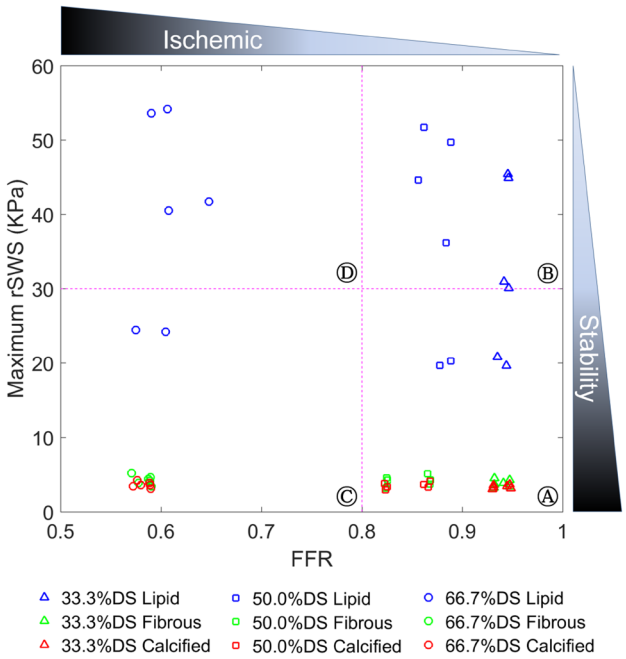

Fig. 5 Simultaneous evaluation of fraction flow reserve (FFR) and maximum relative superficial wall stress (rSWS) of the coronary lesions with four quadrant classification. The smaller the FFR value, the more severe the ischemia; the smaller the maximum rSWS, the more stable the plaque; FFR > 0.80 is non-ischemic (DS% of 33.3% and 50%), FFR ≤ 0.80 is ischemic (DS% of 66.7%); maximum rSWS > 30 kPa is unstable plaque (lipid-rich plaques with positive or no remodeling), maximum rSWS ≤ 30 kPa is stable plaque (fibrous and calcified plaques, and lipid-rich plaques with negative remodeling); Type A: non-ischemic and stable plaque; Type B: non-ischemic and unstable plaque; Type C: ischemic and stable plaque; Type D: ischemic and unstable plaque

and maximum rSWS ≤ 30 kPa) consisted of fibrous or calcified plaques with DS% of 33.3% or 50%, and lipid-rich plaques with DS% of 33.3% or 50% but negative remodeling; Type B: FFR-negative and high maximum rSWS plaques (FFR > 0.80 and maximum rSWS > 30 kPa) included lipid-rich plaques with DS % of 33.3% or 50% but positive or no remodeling; Type C: FFR-positive and low maximum rSWS plaques (FFR ≤ 0.80 and maximum rSWS ≤ 30 kPa) were calcified or fibrous plaques with DS% of 66.7%, and 66.7% diameter narrowing lipid-rich plaques with negative remodeling; and Type D: FFR-positive and high maximum rSWS plaques (FFR ≤ 0.80 and maximum rSWS > 30 kPa) were 66.7% diameter narrowing lipid-rich plaques with positive or no remodeling.

Discussion

We have implemented a new computational model of one-way FSI analysis that allows to simultaneously evaluate both coronary plaque stability and inducible myocardial ischemia. In this study, which comprised a total of 54 FSI analyses in devised idealized stenosis models, we found that both FFR computation and maximum rSWS are affected by a deforming coronary lumen, with higher FFR and maximum rSWS in obstructed coronary segments with lipid-rich plaques. In addition, four types of coronary lesions were further defined based on FFR value and maximum rSWS. This may be useful to identify coronary lesions at a particularly high risk, and it may ultimately help to optimize treatment.

Importantly, FFR values were *higher* (i.e., clinically favorable) in deformable lipid-rich plaques than in rigid fibrous and calcified plaques. This may be explained by the greater cyclic lumen dilatation due to the presence of lipid-rich plaques. As conventional straightforward CFD-computations of FFR typically assume a rigid vessel wall, such methods may in lipid-rich plaques estimate FFR values that actually are too low. Such underestimation of FFR may increase the likelihood of *false-positive* result (i.e., false identification as ischemia-causing) with the risk of performing an invasive treatment that—actually is unjustified from a hemodynamic point of view. Although the mean difference in computed FFR was only 0.02 for stenosis models with different plaque compositions, the difference in individual model might be substantial, e.g., for the 20 mm-long lesion with 50% DS, the difference in computed FFR based on different plaque compositions can be up to 0.07.

Interesting, our results shows that the difference in FFR among three different plaque compositions increased when diameter stenosis increased from 33.3 to 50%, but decreased when diameter stenosis further increased from 50 to 66.7%. This might be explained by the fact that the MLD differed the most between lipid-rich plaque and calcified plaque when the stenosis was moderate. Instead, the MLD differed less when the stenosis became very tight, likely due to the decrease of blood pressure at the radial direction and the increase of blood pressure in the lateral direction, which resulted in less lumen deformation when lipid plaque was presented. We also found that plaques with mild or moderate stenosis and shorter lesion length tended to have higher FFR values than plaques with similar obstruction but longer lesion length. This is consistent with the results of the previous study [22]. The opposite was found for plaques with a severe stenosis (DS% of 66.6%). This could be explained by the conjecture that coronary pressure drop might be related to the longitudinal gradient of the lumen shape. Stroud et al. previously also indicated that the aspect ratio, defined as lesion length divided by lumen diameter, had considerable influence on the flow field [23].

The transient FSI results of the representative example show that the peak rSWS occurs at the lesion's proximal shoulder during systole, whereas the superficial wall produces low stress level during diastole. These findings make sense and are consistent with the results of our previous

study [6]. During early systole, coronary blood flow velocity is slowly decreased and pressure drop through the stenosis is changed mildly (Fig. 3c1–c2), probably because of the extremely high microvascular resistance, caused by the contraction of the ventricle. During late systole, the decrease in coronary pressure drop might be the result of a faster decrease in proximal (aortic) pressure than in distal coronary pressure due to the slowed ventricular ejection. But microcirculatory resistance is still high during the late stage of systole, resulting in a sharp decrease in coronary flow velocity (Fig. 3b2–b3) until the minimum is reached at end-systole due to the closure of the aortic valve. Thereafter, the heart immediately relaxes from the apex and microcirculatory resistance begins to decrease during the early diastole, which may result in a rapid decrease in distal coronary pressure. Thus, pressure drop is markedly increased (Fig. 3c3–c4), which leads to a rapid increase in coronary flow velocity (Fig. 3b4). During late diastole, coronary flow velocity gradually decreases (Fig. 3b4–b1) with the slow decrease in coronary pressure drop (Fig. 3c4–c1), since microcirculatory resistance might be almost invariably in the resting state. In summary, coronary pressure drop and peak flow velocity had a similar trend during the entire cardiac cycle, which is consistent with the empirical formula of the quadratic relationship between pressure drop and flow velocity [17].

In our present study, four types of coronary lesions were categorized, based on different combinations of the maximum rSWS ($>$ or $\leq$ 30 kPa) and FFR ($>$ or $\leq$ 0.80). The group of non-ischemic and stable lesions (Type A), which are quite safe and need no invasive treatment, consisted of hard plaques with a mild-to-moderate stenosis, and lipid-rich plaques with a mild-to-moderate stenosis and negative remodeling. The non-ischemic and unstable lesion group (Type B) consisted of lipid-rich plaques with mild-to-moderate stenosis and without-to-positive remodeling; thus, plaque stability is the primary concern and optimal medical treatment is sufficient while stenting can be safely deferred [24]. The ischemic and stable lesion group (Type C) was hard plaques with a severe stenosis, and lipid-rich plaques with a severe stenosis and negative remodeling; in this group, the ischemia-inducing stenosis is the primary concern and, if technically feasible, there is an indication for coronary stenting. The ischemic and unstable lesion group (Type D) that consists of lipid-rich plaques with severe stenosis and without-to-positive remodeling may be considered as high-risk plaques. Thus, the level of clinical risk increases from Type A to Type B or C, and finally to Type D. Because of the various combinations of vulnerability and hemodynamic significance of coronary lesions, which can also be seen in clinical practice, it makes sense to simultaneously assess plaque vulnerability and inducible ischemia. This may ultimately help to guide and optimize treatment.

In the FAME (fractional flow reserve versus angiography for multivessel evaluation) [25] and FAME II [26] trials, the clinical benefit of FFR-guided PCI was demonstrated. On the other hand, a recent study shows that baseline mechanical plaque stress increased in plaques responsible for MACE and improved the ability of intracoronary imaging to predict events [9]. Of note, Wu et al. [6]. showed several imaging features for identifying vulnerable plaques, such as large lipid core, thin fibrous cap, and positive vessel remodeling, would lead to higher mechanical plaques stress, especially at the superficial wall layer. This supports the potential clinical values of rSWS. Thus, FFR combined with maximum rSWS evaluation of plaque vulnerability may theoretically provide an even better risk stratification and could be useful to choose a tailored treatment strategy, in particular for critical lesions with FFR values between 0.75 and 0.80 (i.e., the 'diagnostic gray zone' of FFR).

The present study has some limitations. Firstly, in all cases the same boundary conditions of pulse pressure at proximal and blood flow velocity at distal were applied. In fact, the hyperemic coronary blood flow velocity may decrease if lumen diameter is reduced by more than 50%, as the counteractive effects of coronary autoregulation are exhausted [27, 28]. However, the assumption of the same boundary conditions of fluid dynamics was deemed acceptable for the purpose of the present comparison. Secondly, we applied the relative pressure field to derive the reasonable wall deformation and stress instead of considering residual stress in the structural analysis. Currently, it is still a great challenge to accurately obtain the residual stress in vivo of atherosclerotic arteries with different composition, morphology and structure. However, in our analysis, the maximum relative SWS of lipid-rich plaques was of the same order of magnitude of the peak stress when considering residual stress in a previous study [18]. Thirdly, composition and morphology of the idealized plaque models differ from actual atherosclerotic plaques. However, the diversity in clinical presentation, substantial inter-individual heterogeneity in circulatory parameters, and the presence of many other confounding factors in real patients have been major obstacles in previous attempts to elucidate the complex biomechanical state of coronary plaques [29]. Therefore, in the present study, simplification of the idealized models was required in order to investigate the effect of individual factors on mechanophysiology indices.

Conclusions

The analysis of fluid–structure interaction to simultaneously evaluate inducible myocardial ischemia and plaque stability may be useful to identify coronary lesions at a high risk and to ultimately optimize treatment. Further research is

warranted to assess whether a more aggressive treatment may improve the prognosis of patients with intermediate, non-ischemic, and unstable lesions.

Funding This study was funded by the National Natural Science Foundation of China (Grant No. 81871460), Program of Shanghai Technology Research Leader, and research programs from Shanghai Jiao Tong University (YG2016ZD09 and YG2015ZD04).

Compliance with ethical standards

Conflict of interest ST has received a research grant from Medis medical imaging and Pulse medical imaging technology. CvB indicated institutional research grants to the research department of TC Twente by Abbott Vascular, Boston Scientific, Biotronik and Medtronic (not related to the present study). XW declares that he has no conflict of interest. SZ declares that she has no conflict of interest. DX declares that she has no conflict of interest. JH declares that she has no conflict of interest.

Ethical approval This article does not contain any studies with human participants or animals performed by any of the authors.

References

1. Taylor CA, Fonte TA, Min JK (2013) Computational fluid dynamics applied to cardiac computed tomography for noninvasive quantification of fractional flow reserve: scientific basis. J Am Coll Cardiol 61(22):2233–2241
2. Van De Hoef TP, Meuwissen M, Escaned J, Davies JE, Siebes M, Spaan JAE, Piek JJ (2013) Fractional flow reserve as a surrogate for inducible myocardial ischaemia. Nat Rev Cardiol 7(8):439–452
3. Pijls NHJ, Tanaka N, Fearon WF (2013) Functional assessment of coronary stenoses: can we live without it? Eur Heart J 34(18):1335–1344
4. Itu L, Rapaka S, Passerini T, Georgescu B, Schwemmer C, Schoebinger M, Flohr T, Sharma P, Comaniciu D (2016) A machine-learning approach for computation of fractional flow reserve from coronary computed tomography. J Appl Physiol 121(1):42–52
5. Tu S, Barbato E, Köszegi Z, Yang J, Sun Z, Holm NR, Tar B, Li Y, Rusinaru D, Wijns W, Reiber JHC (2014) Fractional flow reserve calculation from 3-dimensional quantitative coronary angiography and TIMI frame count. JACC Cardiovasc Interv 7(7):768–777
6. Wu X, von Birgelen C, Li Z, Zhang S, Huang J, Liang F, Li Y, Wijns W, Tu S (2018) Assessment of superficial coronary vessel wall deformation and stress: validation of in silico models and human coronary arteries in vivo. Int J Cardiovasc Imaging 34(2):1–13
7. Kwak BR, Baeck M, Bochaton-Piallat M-L, Caligiuri G, Daemens MJAP, Davies PF, Hoefer IE, Holvoet P, Jo H, Krams R, Lehoux S, Monaco C, Steffens S, Virmani R, Weber C, Wentzel JJ, Evans PC (2014) Biomechanical factors in atherosclerosis: mechanisms and clinical implications. Eur Heart J 35(43):3013–3020
8. Ohayon J, Finet G, Le Floc'h S, Cloutier G, Gharib AM, Heroux J, Pettigrew RI (2014) Biomechanics of atherosclerotic coronary plaque: site, stability and in vivo elasticity modeling. Ann Biomed Eng 42(2):269–279
9. Brown AJ, Teng Z, Calvert PA, Rajani NK, Hennessy O, Nerlekar N, Obaid DR, Costopoulos C, Huang Y, Hoole SP, Goddard M, West NEJ, Gillard JH, Bennett MR (2016) Plaque structural stress estimations improve prediction of future major adverse cardiovascular events after intracoronary imaging. Circ Cardiovasc Imaging 9(6):e004172
10. Holzapfela GA, Mulvihillb JJ, Cunnaneb EM, Walshb MT (2014) Computational approaches for analyzing the mechanics of atherosclerotic plaques: a review. J Biomech 47(4):859–869
11. Akyildiz AC, Speelman L, Gijsen FJH (2014) Mechanical properties of human atherosclerotic intima tissue. J Biomech 47(4):773–783
12. Thondapu V, Bourantas CV, Foin N, Jang I-K, Serruys PW, Barlis P (2016) Biomechanical stress in coronary atherosclerosis: emerging insights from computational modelling. Eur Heart J 38(2):81–92
13. Wu X, von Birgelen C, Muramatsu T, Li Y, Holm NR, Reiber JHC, Tu S (2017) A novel four-dimensional angiographic approach to assess dynamic superficial wall stress of coronary arteries in vivo: initial experience in evaluating vessel sites with subsequent plaque rupture. EuroIntervention 13(9):1099–1103
14. Kock SA, Nygaard JV, Eldrup N, Fründ E-T, Klærke A, Paaske WP, Falk E, Kim WY (2008) Mechanical stresses in carotid plaques using MRI-based fluid-structure interaction models. J Biomech 41(8):1651–1658
15. Teng Zhongzhao, Canton Gador, Yuan Chun, Ferguson Marina, Yang Chun, Huang Xueying, Zheng Jie, Woodard Pamela K, Tang Dalin (2010) 3D critical plaque wall stress is a better predictor of carotid plaque rupture sites than flow shear stress: an in vivo MRI-based 3D FSI study. J Biomech Eng-Trans ASME 132(3):031007
16. Tang D, Yang C, Kobayashi S, Zheng J, Woodard PK, Teng Z, Billiar K, Bach R, Ku DN (2009) 3D MRI-based anisotropic FSI models with cyclic bending for human coronary atherosclerotic plaque mechanical analysis. J Biomech Eng-Trans ASME 131(6):061010
17. Marques KMJ, Spruijt HJ, Boer C, Westerhof N, Visser CA, Visser FC (2002) The diastolic flow-pressure gradient relation in coronary stenoses in humans. J Am Coll Cardiol 39(10):1630–1636
18. Ohayon J, Dubreuil O, Tracqui P, Le Floc'h S, Rioufol G, Chalabreysse L, Thivolet F, Pettigrew RI, Finet G (2007) Influence of residual stress/strain on the biomechanical stability of vulnerable coronary plaques: potential impact for evaluating the risk of plaque rupture. A J Physiol-Heart Circ Physiol 293(3):H1987–H1996
19. Wolf K, Bayrasy P, Brodbeck C, Kalmykov I, Oeckerath A, Wirth N (2017) MpCCI neutral interfaces for multiphysics simulations. Springer, New York
20. Young DF, Cholvin NR, Kirkeeide RL, Roth AC (1977) Hemodynamics of arterial stenoses at elevated flow rates. Circ Res 41(1):99–107
21. Costopoulos C, Huang Y, Brown AJ, Calvert PA, Hoole SP, West NEJ, Gillard JH, Teng Z, Bennett MR (2017) Plaque rupture in coronary atherosclerosis is associated with increased plaque structural stress. JACC Cardiovasc Imaging 10:1472
22. Chu M, von Birgelen C, Li Y, Westra J, Yang J, Holm NR, Reiber JHC, Wijns W, Tu S (2018) Quantification of disturbed coronary flow by disturbed vorticity index and relation with fractional flow reserve. Atherosclerosis 273:136–144
23. Stroud JS, Berger SA, Saloner D (2000) Influence of stenosis morphology on flow through severely stenotic vessels: implications for plaque rupture. J Biomech 33(4):443–455
24. Pijls NHJ, Sels J-W (2012) Functional measurement of coronary stenosis. J Am Coll Cardiol 59(12):1045–1057
25. Tonino PAL, De Bruyne B, Pijls NHJ, Siebert U, Ikeno F, vant Veer M, Klauss V, Manoharan G, Engstrøm T, Oldroyd KG, Ver Lee PN, Maccarthy PA, Fearon WF (2009) Fractional flow reserve versus angiography for guiding percutaneous coronary intervention. N Engl J Med 360(3):213–224

26. De Bruyne B, Pijls NHJ, Kalesan B, Barbato E, Tonino PAL, Piroth Z, Jagic N, Möbius-Winkler S, Rioufol G, Witt N, Kala P, MacCarthy P, Engström T, Oldroyd KG, Mavromatis K, Manoharan G, Verlee P, Frobert O, Curzen N, Johnson JB, Jüni P, Fearon WF (2012) Fractional flow reserve–guided PCI versus medical therapy in stable coronary disease. N Engl J Med 367(11):991–1001
27. Mosher P, Ross J, Mcfate PA, Shaw RF (1964) Control of coronary blood flow by an autoregulatory mechanism. Circ Res 14(3):250–259
28. Hoffman JIE (2000) Problems of coronary flow reserve. Ann Biomed Eng 28(8):884–896
29. Choi G, Lee JM, Kim HJ, Park JB, Sankaran S, Otake H, Doh JH, Nam CW, Shin ES, Taylor CA (2015) Coronary artery axial plaque stress and its relationship with lesion geometry: application of computational fluid dynamics to coronary CT angiography. JACC Cardiovasc Imaging 8(10):1156–1166